Optica Applicata, Vol. XLV, No. 1, 2015
DOI: 10.5277/oa150103

Polarity-reversed ultra-wideband monocycle pulse generation with dual-channel multicasting in a photonic crystal fiber

JIAMIN GONG, ZHANQIANG HUI*

Xi'an University of Posts and Telecommunications, Xi'an 710121, China

*Corresponding author: zhanqianghui@xupt.edu.cn

This paper proposes and demonstrates a novel scheme of a two-channel-output ultra-wideband monocycle pulse generator consisting of a 100 m dispersion-flattened highly nonlinear photonic crystal fiber and two optical bandpass filters. Based on the cross-phase modulation effect in a dispersion-flattened highly nonlinear photonic crystal fiber, two polarity-reversed ultra-wideband monocycle pulses simultaneously output from two different channels are successfully achieved by appropriately locating the probe wavelength at the left linear slope and the right linear slope of the two optical bandpass filters transmission spectra, respectively. The full width at half-maximum and a fractional bandwidth of 24 ps and 260% for a positive pulse, 24 ps and 251% for a negative pulse are obtained. Moreover, the influences of input signal powers, the polarization misalignment between the data light and the continuous wave probe light, and probe wavelength variation on the double output ultra-wideband signals quality are also investigated. The results show that the system has some tolerance to both the input signal power fluctuation and the slight polarization mismatch and even can efficiently operate with a widely tunable wavelength range. This makes it very attractive for engineering applications in future multiuser ultra-wideband-over-fiber communication systems.

Keywords: nonlinear optics, cross-phase modulation (XPM), radio frequency photonics, ultra-wideband (UWB), photonic crystal fiber (PCF).

1. Introduction

Ultra-wideband (UWB) is a promising technology for short-range high-speed wireless communications and sensor networks owing to its advantages including low power consumption, high immunity to multipath fading, enhanced penetration capability, large bandwidth and high data rates under unlicensed spectrum from 3.1 to 10.6 GHz [1]. However, with the low power spectral density prescribed by the Federal Communications Commission (FCC), the operation range of UWB signal is limited to the immediate area (up to tens of meters). To avoid such short-range networks operating only

in a stand-alone mode, UWB-over-fiber technology has been proposed as a very promising solution to integrate local UWB environment into the fixed wired networks or wireless wide-area infrastructures by taking advantage of low loss and extremely broad bandwidth offered by the optical fiber [2]. Then, the generation of UWB signals directly in the optical domain avoiding the extra optical–electrical and electrical–optical conversion has received considerable attention. Among the many UWB pulses, Gaussian monocycle is considered as an excellent candidate for UWB impulse communications due to the simplicity and achievability in generating this pulse. So far, many approaches have been reported to optically generate UWB monocycle pulses, such as using cross-gain modulation [3], cross-phase modulation [4] in a semiconductor optical amplifier (SOA); based on relaxation oscillations of a semiconductor laser [5]; based on a gain-switched semiconductor laser with optical feedback [6]; using cross-absorption modulation in an electro-absorption modulator (EAM) [7]; using sum-frequency generation in a PPLN waveguide [8]; using a nonlinear optical loop mirror (NOLM) [9–11], Mach–Zehnder interferometer [12], delay interferometer [13] or Sagnac interferometer [14]; using a reconfigurable photonic microwave delay-line filter [15]; using a dual-parallel [16] or cascaded Mach–Zehnder modulator (MZM) [17]; using a high-speed electro-optic phase modulator and a fiber-Bragg-grating-based frequency discriminator [18]; based on an optical carrier phase-shifting technique by cascading polarization modulators (PolMs) [19]; using pulse compression [20], cross-phase modulation (XPM) [21–23], four-wave mixing [24] and gain saturation [25] in a highly nonlinear fiber (HNLF); using XPM in a bismuth-oxide-based nonlinear optical fiber (Bi-NLF) [26] or in a chalcogenide waveguide [27]; using a photonic chip composed of a silicon micro-ring resonator [28] or silicon nitride waveguide [29]; and using spectral shaping and dispersion-induced frequency-to-time conversion [30].

All these methods show an impressive operation performance, and also have respective advantages and drawbacks. For example, the output signal shape highly depends on the input signal polarization state in NOLM, and a relatively long gain recovery time in SOA or EAM ultimately limits their operating performance. Moreover, the interferometer-based devices usually have a complicated structure and sometimes require temperature control; and the high manufacturing cost for micro-ring resonators, photonic chips and various novel bismuth-oxide-based optical fibers or chalcogenide waveguides may prevent them from being applied in practice. Some others are also very sensitive to the surrounding environment. Meanwhile, the necessity of placing the pump wavelength near the zero-dispersion wavelength of a DSF arises to ensure phase matching. This might limit the operation flexibility of a UWB signal generator. Moreover, the relatively low nonlinearity of the DSF generally requires using the fiber length even up to several kilometers in practical applications. The temporal distortion of the generated pulse shape usually is related to the beam stability problem caused by the great length of the DSF. Recently, dispersion-flattened highly nonlinear photonic crystal fibers (DF-HNL-PCFs) have been employed for all optical signal processing because of their unique properties such as the high nonlinear coefficient and controllable dispersion profile [31, 32].

In this paper, we propose and demonstrate a polarity-reversed UWB monocycle pulses generator with a function of dual-channel multicasting by using XPM in a DF-HNL-PCF. The system is composed of a 100-m DF-HNL-PCF and two optical bandpass filters (OBPFs). The positive and negative polarity UWB monocycle pulses are simultaneously acquired, which can be transmitted to different users in UWB over the fiber system. Moreover, pulse polarity modulation (PPM) to UWB optical pulse can be conveniently realized. Furthermore, the influence of an input signal power, wavelength separation, and polarization mismatch between signal and probe lights on the quality of the generated UWB pulses are also investigated. To our knowledge, it is the first report about the dynamic characteristics of designed DF-HNL-PCF based UWB monocycle pulse generator, which demonstrates that the generated UWB monocycle pulses have advantages of a simple structure, high extinction ratio, efficient operation with a wide wavelength range, and good tolerance to system parameter fluctuations, which has potential applications in multiuser UWB-over-fiber communication systems.

2. Operating principle

The operation principle of the proposed polarity-reversed UWB monocycle pulse photonic generator is shown in Fig. 1, which comprises an optical coupler (OC), an optical splitter (OS), a 100-m DF-HNL-PCF, and two OBPFs. Optical RZ data signals of frequency ν_{signal} and power P_{signal} and continuous wave (CW) of frequency ν_{cw} and power P_{cw} are combined by a 2×1 optical power combiner, and then they are launched into the DF-HNL-PCF. In general, the injected optical RZ data pulses with sufficiently high peak power propagate in a nonlinear medium (*i.e.*, DF-HNL-PCF) and lead to a refractive-index change of the DF-HNL-PCF via the optical Kerr effect. This causes a nonlinear phase shift of the co-propagating CW probe light via XPM, and therefore, generates both temporal red and blue chirps on two sides of the probe light, which is the first-order derivative of the phase variation. The chirp is the frequency shift of the probe signal, and its positive or negative value represents blue-shift

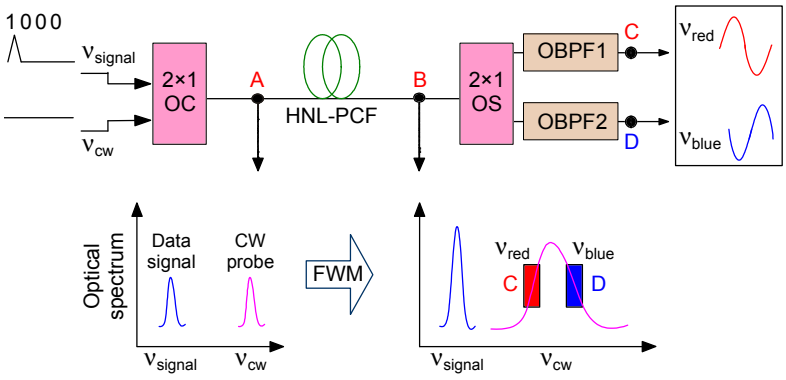

Fig. 1. Operation principle of the HNL-PCF-based polarity-reversed UWB monocycle pulse generator.

or red-shift of the probe wavelength, respectively. Owing to the symmetry of the OBPF transfer function, the output pulse will be a monocycle shape with a π phase difference when the probe carrier is located at the left linear slope and the right linear slope of the filter transmission spectrum (point *C* and *D* in Fig. 1) [33]. Then, a pair of polarity--reversed UWB monocycle pulses can be simultaneously obtained and distributed to different users through fiber links from different OBPF channel. Since the UWB pulses of different shapes (positive and negative) can be generated, they have the potential to realize PPM in multiuser UWB-over-fiber communication systems.

3. Simulation and results

Figure 1 shows a schematic diagram of all-optical multiuser UWB communication systems using the DF-HNL-PCF based XPM effect and OBPF-based frequency discriminator. In the central station (CS), tuneable laser TL1 emits CW light located at 1561.5 nm, which is modulated by a MZM to form optical Gaussian pulses, and a bit pattern generator (BPG) drives the MZM at a repetition rate of 10 Gb/s with a fixed pattern "1000 0000 0000 0000" (one "1" per 16 bits), which is equivalent to a Gaussian pulse train with a repetition rate of 0.625 GHz. The CW probe light with the central wavelength at λ_{cw} = 1556.52 nm is produced by another wavelength tunable laser (TL2, see Fig. 2). The RZ data signal light and CW probe light are combined by a 2×1 OC, and are launched into a DF-HNL-PCF. In this case, the DF-HNL-PCF acts as a nonlinear element to broaden the spectrum of input CW probe light due to the XPM effect. Two linear polarizers (LP1 and LP2, see Fig. 2) are used to adjust the polarization states of both RZ data signal and CW probe lights to optimize the XPM effect between them. At the DF-HNL-PCF output port, two central wavelength-tunable OBPFs are employed in parallel at the output of a 1×2 OS. If the probe light is simultaneously aimed to left and right linear slopes of two OBPFs transmittance curves, the positive and negative polarity UWB monocycle pulses are simultaneously acquired at the out ports of the two according channels. Generated UWB signals are distributed to base stations (BSs) through fiber links from different OBPF channels. BS is formed by a PIN photodetector (PIN-PD) and a power amplifier (PA), in which an optical signal is converted into an electrical signal, and is monitored by a high-speed oscilloscope and an electrical spectrum analyzer (ESA).

In the simulation, the DF-HNL-PCF parameters are set as follows: length 100 m, effective area 8 μm^2, nonlinear refractive coefficient 2.6×10^{-20} $m^2\cdot W^{-1}$, internal loss 9 $dB\cdot km^{-1}$, dispersion parameter *D* is 0.5 $ps\cdot nm^{-1}\cdot km^{-1}$, the third-order dispersion (TOD) is 0.001 $ps\cdot nm^{-2}\cdot km^{-1}$. Moreover, the differential group delay is set as 0.5 $ps\cdot km^{-1}$. Those are all consistent with the commercially available product of DF-HNL-PCF. This DF-HNL-PCF has a high index. The difference between the silica and air-filled hole enables the tight mode confinement resulting in a small effective area, controllable dispersion profile and a high nonlinear coefficient [32]. Then, due to a high nonlinear coefficient and flattened dispersion in DF-HNL-PCF, we can easily

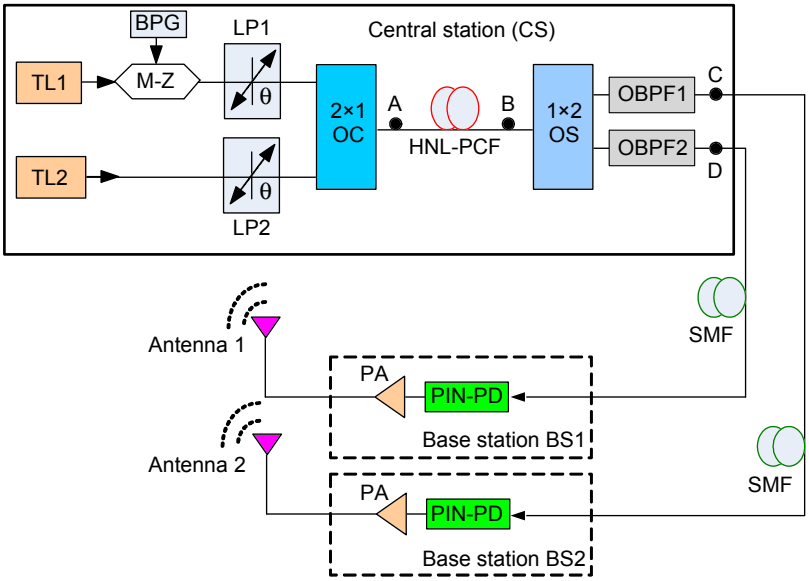

Fig. 2. Simulation setup of the dual-channel output polarity-reversed UWB monocycle pulse generator exploiting XPM in a HNL-PCF. BPG – bit pulse generator, TL – tunable laser, M-Z – Mach–Zehnder modulator, LP – linear polarizer, OC – optical coupler, OS – optical splitter, OBPF – optical bandpass filter, HNL-PCF – highly nonlinear photonic crystal fiber, PIN-PD – PIN-photoelectric detector, PA – power amplifier.

obtain the evident XPM effect with a widely tunable wavelength range using short fiber length of only 100 m.

Two LPs are employed to adjust the polarization states of both RZ data and CW lights in order to maximize the XPM efficiency between them in the DF-HNL-PCF. Moreover, the tunable lasers with tunable output power are used to ensure that data and probe lights have sufficient optical powers to feed into the HNL-PCF. The input data signal is 10 Gbit/s pulse trains at 1561.5 nm with pattern "1000 0000 0000 0000". The optical power for the data signal and probe light launched into the HNL-PCF is 28 dB·m and 10 dB·m, respectively. The duty cycle of an input pulse is 0.1. The simulation results of polarity-reversed UWB monocycle pulses generation based on XPM are obtained. The optical spectra before HNL-PCF, after HNL-PCF, after OBPF1 and after OBPF2 (corresponding to *A*, *B*, *C* and *D* in Fig. 2) are recorded by an optical spectrum analyzer and shown in Fig. 3. It can be seen that there is little spectrum overlap between data light at 1561.5 nm and CW light at 1556.52 nm. It should be noted that an evident characteristics in Fig. 3**b** is that the spectra of CW beam are broadened after HNL-PCF, which is induced by XPM from data signal with high peak power. Although the FWM is inevitable and coexists with the XPM in the DF-HNL-PCF, the XPM could remain dominant when $\Delta\lambda_{\text{det}} = \lambda_{\text{cw}} - \lambda_{\text{OBPF}}$ is rather small. Therefore the contribution of the FWM is negligible and beyond the scope in our proposed scheme. At the DF-HNL-PCF

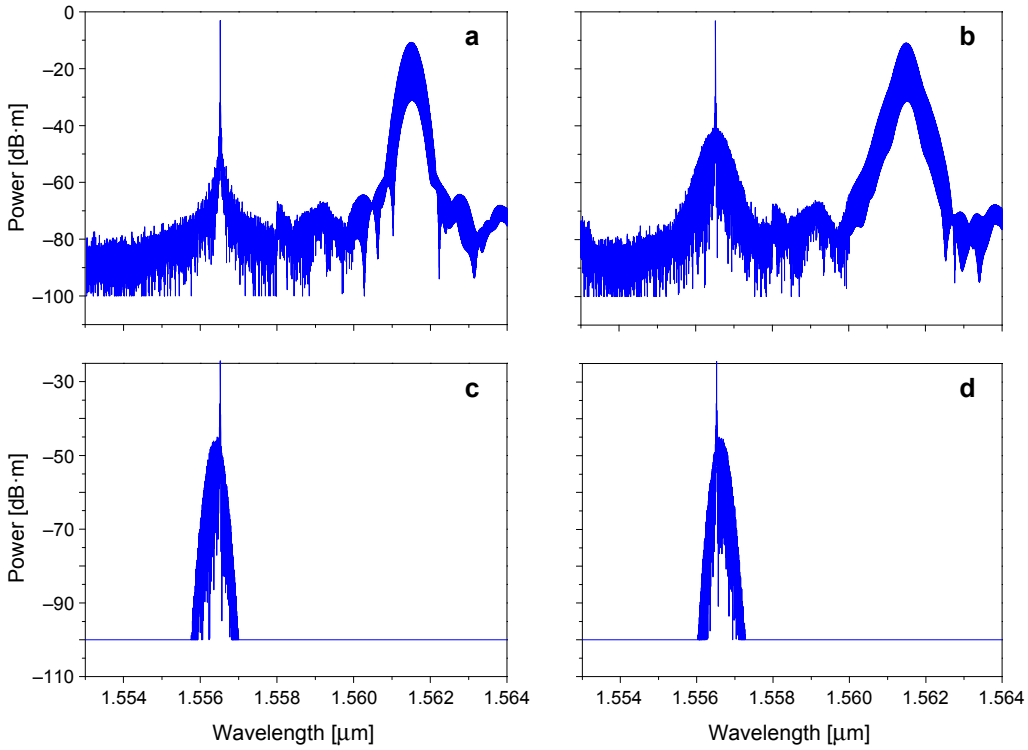

Fig. 3. Optical spectra for the dual-channel output polarity-reversed UWB monocycle pulse generator, before HNL-PCF (**a**), after HNL-PCF (**b**), after OBPF1 (**c**) and after OBPF2 (**d**).

output, we use two sets of tunable OBPFs (*i.e.*, OBPF1 and OBPF2 in Fig. 2) with a 3-dB bandwidth of 0.3 nm to exact the chirp components with different polarity, which are the output positive and negative polarity UWB monocycle pulses of the designed photonic UWB pulse generator.

The measured temporal waveforms and electrical spectra of the acquired UWB monocycle pulses are shown in Fig. 4. Figure 4**a** depicts the waveform of the positive polarity UWB monocycle pulse. The upper full-width at half maximum (FWHM) and the lower FWHM are 24 and 23.5 ps, respectively. Figure 4**b** shows that the corresponding electrical spectrum has a central frequency of 8.44 GHz and a 10-dB bandwidth of 20.3 GHz, thus, the fractional bandwidth is 240%. Figures 4**c** and 4**d** show the waveform and electrical spectrum of the obtained negative polarity UWB monocycle pulse, respectively. The upper FWHM and the lower FWHM are 24 and 23.8 ps, respectively. The central frequency is 8.44 GHz with a 10-dB bandwidth of 20.74 GHz, thus, the fractional bandwidth is 246%. The two monocycle pulses have different polarity. The difference is determined by the linear slope of a filter transmission spectrum. Both of the two UWB signals with different pulse polarity have an electrical spectrum that agrees well with the regulations established by FCC. The frequency spacing be-

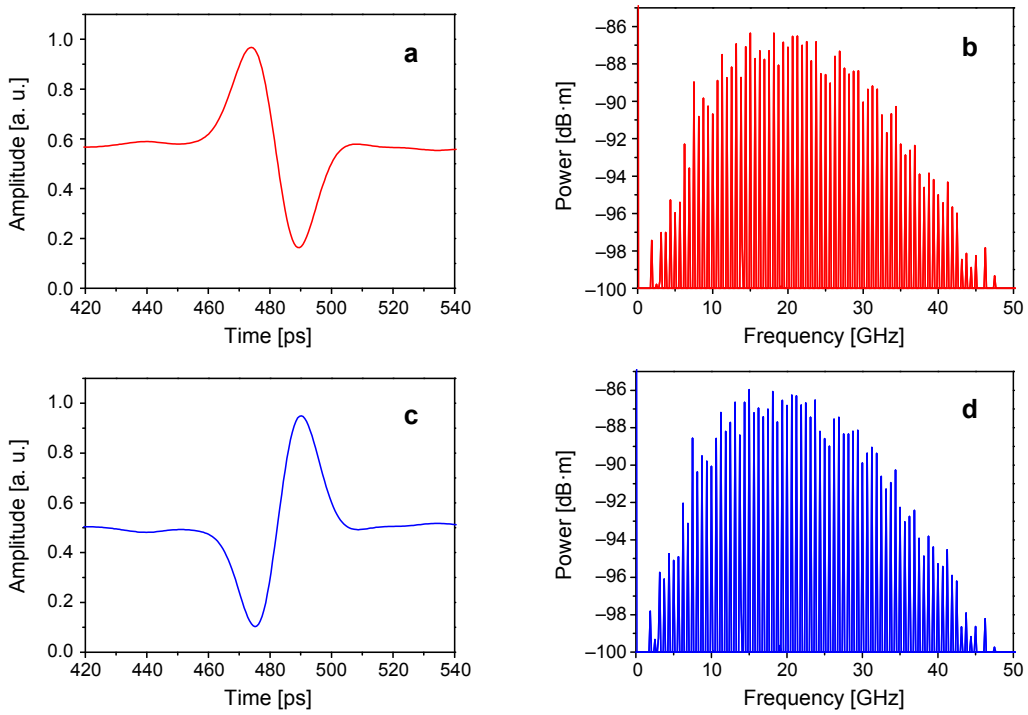

Fig. 4. Measured waveforms and electrical spectra of the acquired inverted polarity UWB monocycle pulses in two channels, waveform (**a**) and RF spectrum (**b**) for a positive polarity UWB monocycle pulse, and waveform (**c**) and RF spectrum (**d**) for a negative polarity UWB monocycle pulse.

tween two neighboring lines is measured to be 0.625 GHz, which is equal to the repetition rate of the monocycle pulse train. Theoretically, the maximum repetition rate is limited by the response time of the Kerr effect, which is usually in the range of a femtosecond. Therefore, the maximum repetition rate is about terabits per second, which is much higher than the data rate of 100–200 Mbits/s required by the UWB technology.

4. Discussions

In practical UWB-over-fiber communication systems, the power and polarization state of signal lights can be changed in an occasional and random fashion, which will degrade the performance of UWB pulses and increase the power penalty of UWB-over-fiber networks. From the viewpoint of engineering applications, the tolerance to changes of the parameters, such as optical power, polarization state, *etc*., is an important issue in the design of a photonic UWB pulse generator. As far as we know, this is the first time to discuss how the parameters affect the performance of UWB pulse quality based on XPM in a HNL-PCF. Because of simple configuration of our designed photonic

UWB pulse generator, only a few parameters will influence its performance, such as the injected powers of signal lights, the polarization state fluctuation of signal lights, and the wavelength separation between the signal and probe lights.

In this part, we will show the photonic UWB pulse generator output results when the operation parameters are changed, such as the input power of signal lights, polarization misalignment of signal lights. Then we discuss how to improve the UWB pulse generator output signal quality by optimizing all the above mentioned parameters. Moreover, the impact of wavelength separation variation between signal and CW probe lights is also investigated. Then, we try to optimize the photonic UWB pulse generator output based on those results.

4.1. The input power of data signal

For practical UWB-over-fiber communication application, the power variation of the signal light cannot be avoided completely due to the random change of system operation conditions. Then, the polarity-reversed UWB monocycle pulse generator with multicasting capabilities should show some tolerance to the input signal power fluctuation. In our simulation, we test the performance of the designed UWB monocycle pulse generator with different input power while maintaining other parameters constant to make the results comparable. In this case, the wavelengths of signal and CW probe light are 1561.5 and 1556.52 nm, respectively. The HNL-PCF length and the CW probe power are 100 m and 10 dB·m. The signal power is varied from 24 to 30 dB·m in a step of 1 dB. The input spectrum (before HNL-PCF) is shown in the frontier of Fig. 5 for comparison. It can be seen that when the signal light power is increased, the XPM-induced CW probe spectrum is broadened, which indicates the degree of phase modulation increase with the increase in input signal light power significantly. The FWHM and fractional bandwidth from an oscilloscope and ESA are measured and

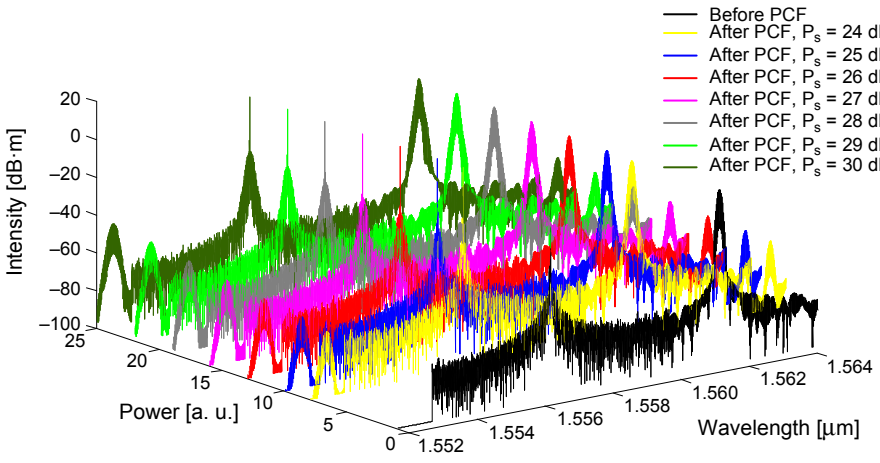

Fig. 5. Spectra at the output of a HNL-PCF when λ_s = 1561.5 nm, λ_{cw} = 1556.52 nm, P_{cw} = 10 dB·m, P_s = 24, 25, 26, 27, 28, 29 and 30 dB·m, respectively.

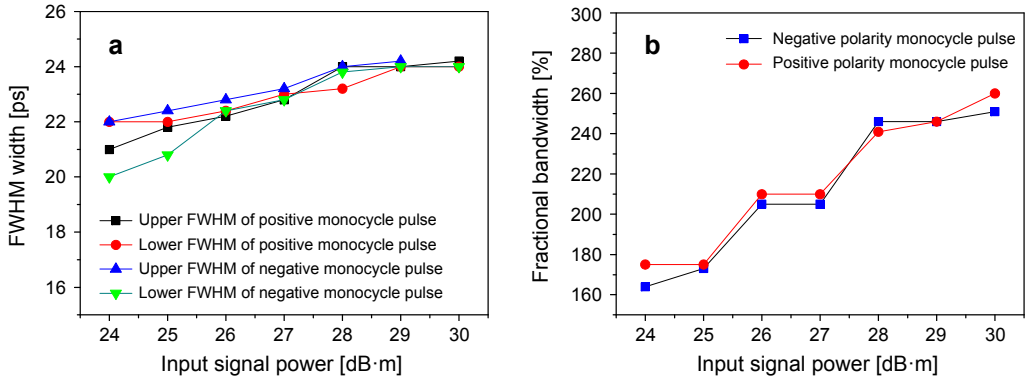

Fig. 6. The FWHM (**a**) and fractional bandwidth (**b**) for the generated monocycle pulses under different input signal power.

plotted as a function of input signal light power for a positive polarity pulse and a negative polarity pulse, and are shown in Figs. 6**a** and 6**b**, respectively. Generally, we can see that FWHM is increasing slowly while fractional bandwidth is increasing obviously, and then there is little change with the increase in input power. It can be contributed to the variation in phase modulation induced by signal power.

4.2. The polarization misalignment of data signal lights

XPM is polarization dependent because it involves the interaction of several optical waves. As far as a XPM based photonic UWB monocycle pulse generator is concerned, the polarization dependence can cause a major problem for engineering applications. This is because the polarization state of data signal light is normally unknown at the input port of an optical receiver after practical optical fiber transmission and can be changed randomly over time due to varying system operation conditions/environment. From the point of view of engineering applications, to pave the way of using a HNL-PCF based UWB monocycle pulse generator with PPM capabilities in UWB-over-fiber communication systems, it is necessary to investigate the effect of polarization states of data signal lights on the positive and negative polarity monocycle pulses at the HNL-PCF based UWB monocycle pulse generator.

In this case, the wavelengths of signal and CW probe light are 1561.5 nm and 1556.52 nm, respectively. The signal light power is 30 dB·m. The other parameters are all the same as before. In the simulation, we vary the polarization state of the signal light while maintaining the other parameters unchanged to make the results comparable. We can see that the spectral broadening degree is varying with the change of a signal polarization state. Two typical waveform diagrams of positive and negative monocycle pulses for a polarity mismatch angle of 0° and 50° are recorded and shown in Figs. 7**a** and 7**b**. Then, we can find that the generated UWB pulse signal quality degrades severely with the increase of the polarization mismatch angle θ from 0° to 50°. When θ exceeds 50°, the degradation of signal quality becomes rapid and we even

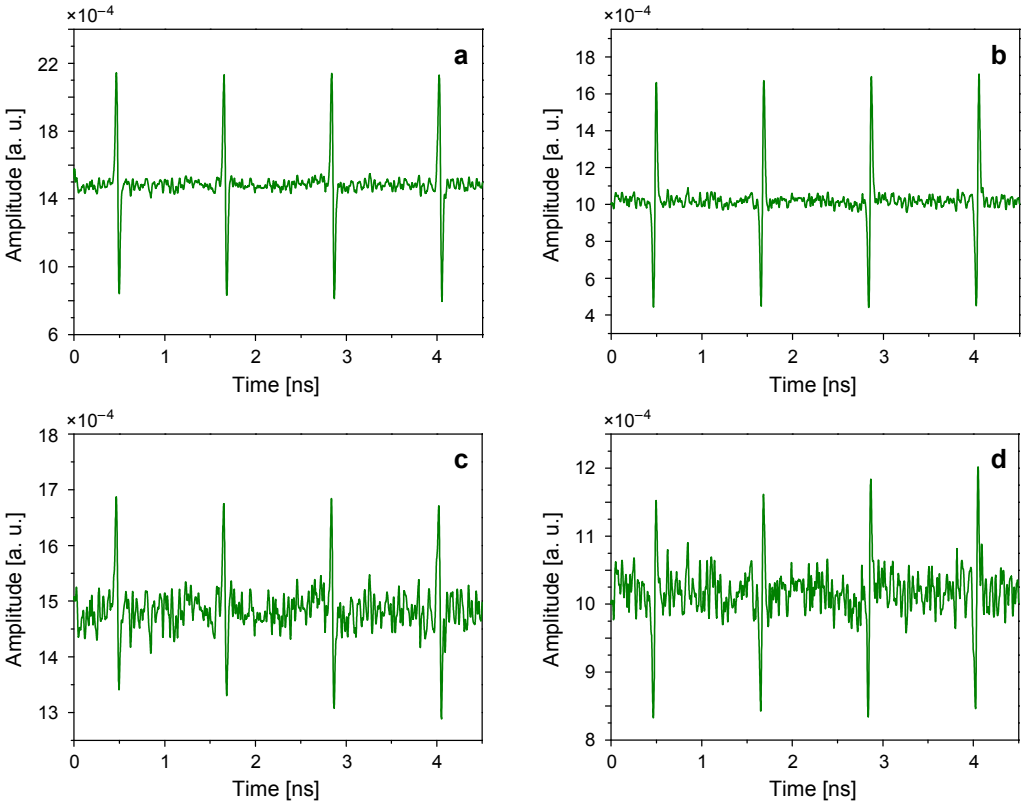

Fig. 7. Waveform diagrams of positive polarity monocycle pulse for $\theta = 0°$ (**a**) and negative polarity monocycle pulse for $\theta = 0°$ (**b**), positive polarity monocycle pulse for $\theta = 50°$ (**c**) and negative polarity monocycle pulse for $\theta = 50°$ (**d**).

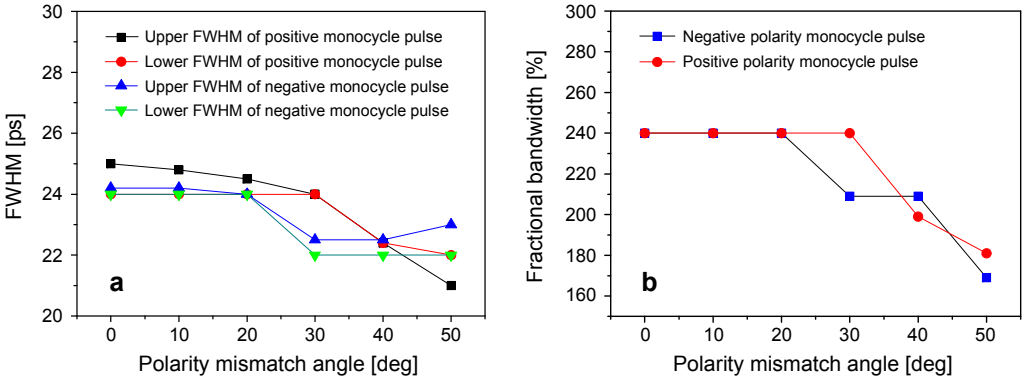

Fig. 8. The FWHM (**a**) and fractional bandwidth (**b**) for the generated monocycle pulses under different polarization mismatch angles.

cannot obtain the available UWB pulse. Then, it can be concluded that our designed photonic UWB monocycle pulse generator with multicasting capabilities is sensitive to the polarization of signal light. Furthermore, the FWHM and fractional bandwidth are measured and plotted as a function of a polarization mismatch angle for a positive polarity pulse and negative polarity pulse, and are shown in Figs. 8**a** and 8**b**, respectively. Generally speaking, we can see that the FWHM and fractional bandwidth are all decreasing slowly with the increase in input power. It can be contributed to the decrease in valid input signal power that plays a key role for phase modulation.

4.3. The variation of wavelength separation

In practical UWB-over-fiber communication systems, a photonic device with a wide operating wavelength range is highly desirable for engineering applications [34–38], especially for a photonic UWB pulse generator, which can be used to reduce the probability of wavelength blocking and to enhance the wavelength routing capability in large capacity UWB-over-fiber WDM networks. Hence, we carry out a systematic investigation into the wavelength tunability of the designed HNL-PCF based UWB pulse generator. In this simulation, the CW probe light with different central wavelength is obtained by using a wavelength tunable laser. The tuning characteristics of the HNL-PCF based UWB pulse generator is measured by varying the input signal light wavelength. Due to the operation range of commercially available EDFA which is usually in C-band (from 1530 nm to 1565 nm), we vary the wavelength of CW probe light from 1530 nm to 1565 nm in a step of 1 nm. Some typical optical spectra of XPM in HNL-PCF based UWB monocycle pulses generator are illustrated in Figs. 9**a**–9**d** with CW probe wave-

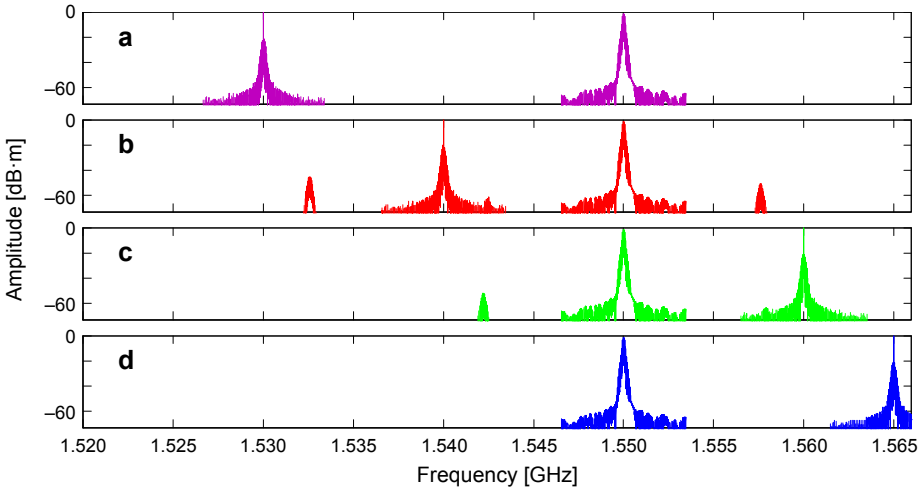

Fig. 9. Optical spectra for the dual-channel output polarity-reversed UWB monocycle pulse generator, λ_{signal} = 1550 nm, and λ_{cw} = 1530 nm (**a**), λ_{cw} = 1540 nm (**b**), λ_{cw} = 1560 nm (**c**), λ_{cw} = 1565 nm (**d**).

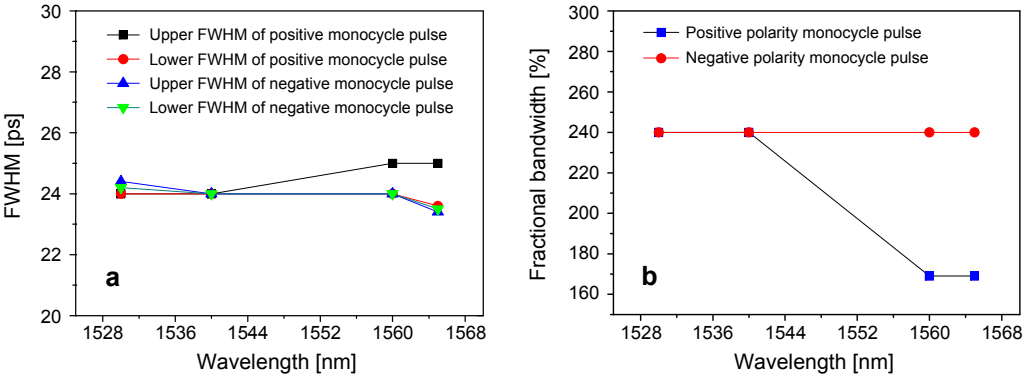

Fig. 10. The FWHM (**a**) and fractional bandwidth (**b**) for the generated monocycle pulse under different probe light wavelengths.

length at 1530, 1540, 1560 and 1565 nm, respectively. It can be seen that the CW probe spectrum is broadened evidently by signal light with high peak power in all measured wavelengths. Corresponding positive and negative polarity monocycle pulses with a good extinction ratio are also acquired and shown in Fig. 10. The results indicate that our designed all-optical UWB pulse generator can achieve a wide operating wavelength range in the whole C-band.

5. Conclusions

In summary, we have proposed and demonstrated a novel polarity-reversed photonic UWB monocycle pulse generator with a dual-channel output that consists of a single 100 m DF-HNL-PCF and two OBPFs. The UWB monocycle pulse generator is based on spectral broadening of the input probe light due to the XPM in the DF-HNL-PCF and subsequent phase to intensity conversion. The positive polarity and negative polarity monocycle pulses are simultaneously obtained with the optimum FWHM and fractional bandwidth of 24 ps and 260%, 24 ps and 250%, respectively. Furthermore, we have systematically investigated the dynamic characteristics and wavelength tunability of the designed UWB monocycle pulse generator by varying the injected power of the input RZ data signal and the central wavelengths of the CW probe light. It has been shown that the designed scheme has some tolerance to both the input signal power fluctuation and the slightly polarization mismatch, and has a widely tunable wavelength range in the whole C-band. Moreover, the resulting configuration is a simple, robust, ultrafast response and all-fiber based, which shows that it has potential engineering applications in future multiuser UWB-over-fiber communication systems.

Acknowledgements – This work is supported by the National Nature Science Fund of China (no. 61201193), the National High Technology Research and Development Program of China (no. 2013AA014504),

the Foundation of Shaanxi Educational Committee (no. 2013JK1094), the Shaanxi Province Science and Technology Research and Development Program (no. 2014k05-40), and the Youth Foundation of Xi'an University of Posts and Telecommunications (no. 105-1209).

References

[1] JIANPING YAO, FEI ZENG, QING WANG, *Photonic generation of ultrawideband signals*, Journal of Lightwave Technology **25**(11), 2007, pp. 3219–3235.

[2] SHILONG PAN, JIANPING YAO, *UWB-over-fiber communications: modulation and transmission*, Journal of Lightwave Technology **28**(16), 2010, pp. 2445–2455.

[3] QING WANG, FEI ZENG, BLAIS S., JIANPING YAO, *Optical ultrawideband monocycle pulse generation based on cross-gain modulation in a semiconductor optical amplifier*, Optics Letters **31**(21), 2006, pp. 3083–3085.

[4] JIANJI DONG, XINLIANG ZHANG, JING XU, DEXIU HUANG, SONGNIAN FU, SHUM P., *Ultrawideband monocycle generation using cross-phase modulation in a semiconductor optical amplifier*, Optics Letters **32**(10), 2007, pp. 1223–1225.

[5] XIANBIN YU, BRAIDWOOD GIBBON T., PAWLIK M., BLAABERG S., TAFUR MONROY I., *A photonic ultra--wideband pulse generator based on relaxation oscillations of a semiconductor laser*, Optics Express **17**(12), 2009, pp. 9680–9687.

[6] MINGJIANG ZHANG, MING LIU, ANBANG WANG, YONGNING JI, ZHE MA, JUNFENG JIANG, TIEGEN LIU, *Photonic generation of ultrawideband signals based on a gain-switched semiconductor laser with optical feedback*, Applied Optics **52**(31), 2013, pp. 7512–7516.

[7] MO LI, WEI DONG, JINGRAN ZHOU, CAIXIA LIU, XINDONG ZHANG, SHENGPING RUAN, WEIYOU CHEN, *Photonic generation of ultrawideband doublet pulse based on cross-absorption modulation in an electroabsorption modulator*, Strait Quad-Regional Radio Science and Wireless Technology Conference (CSQRWC), Vol. 1, 2011, pp. 278–280.

[8] JIAN WANG, QIZHEN SUN, JUNQIANG SUN, WEIWEI ZHANG, *All-optical UWB pulse generation using sum-frequency generation in a PPLN waveguide*, Optics Express **17**(5), 2009, pp. 3521–3530.

[9] TIANYE HUANG, JIA LI, JUNQIANG SUN, CHEN L.R., *Photonic generation of UWB pulses using a nonlinear optical loop mirror and its distribution over a fiber link*, IEEE Photonics Technology Letters **23**(17), 2011, pp. 1255–1257.

[10] TIANYE HUANG, JIA LI, JUNQIANG SUN, CHEN L.R., *All-optical UWB signal generation and multicasting using a nonlinear optical loop mirror*, Optics Express **19**(17), 2011, pp. 15885–15890.

[11] BOWEN LUO, TING YANG, JIANJI DONG, YUAN YU, DEXIU HUANG, XINLIANG ZHANG, *All-optical millimeter-wave ultrawideband signal generation using a nonlinear optical loop mirror*, IEEE Photonics Journal **4**(2), 2012, pp. 350–356.

[12] BEN EZRA Y., HARIDIM M., LEMBRIKOV B.I., RAN M., *Proposal for all-optical generation of ultra-wideband impulse radio signals in Mach–Zehnder interferometer with quantum-dot optical amplifier*, IEEE Photonics Technology Letters **20**(7), 2008, pp. 484–486.

[13] FEI WANG, EN-MING XU, *All-optical UWB doublet pulses generation by using a delay interferometer*, Optics Communications **297**, 2013, pp. 38–42.

[14] JIANQIANG LI, KUN XU, SONGNIAN FU, JIAN WU, JINTONG LIN, MING TANG, SHUM P., *Ultra-wideband pulse generation with flexible pulse shape and polarity control using a Sagnac interferometer-based intensity modulator*, Optics Express **15**(26), 2007, pp. 18156–18161.

[15] QING WANG, JIANPING YAO, *Switchable optical UWB monocycle and doublet generation using a reconfigurable photonic microwave delay-line filter*, Optics Express **15**(22), 2007, pp. 14667–14672.

[16] FANGZHENG ZHANG, SHILONG PAN, *Background-free millimeter-wave ultra-wideband signal generation based on a dual-parallel Mach–Zehnder modulator*, Optics Express **21**(22), 2013, pp. 27017–27022.

[17] YUAN YU, JIANJI DONG, XIANG LI, XINLIANG ZHANG, *Ultra-wideband generation based on cascaded Mach–Zehnder modulators*, IEEE Photonics Technology Letters **23**(23), 2011, pp. 1754–1756.

[18] FEI ZENG, JIANPING YAO, *Ultrawideband impulse radio signal generation using a high-speed electro-optic phase modulator and a fiber-Bragg-grating-based frequency discriminator*, IEEE Photonics Technology Letters **18**(19), 2006, pp. 2062–2064.

[19] WEI LI, LI XIAN WANG, JIAN YU ZHENG, MING LI, NING HUA ZHU, *Photonic generation of ultra-wideband signals with large carrier frequency tunability based on an optical carrier phase-shifting method*, IEEE Photonics Journal **5**(5), 2013, article 5502007.

[20] ZADOK A., XIAOXIA WU, SENDOWSKI J., YARIV A., WILLNER A.E., *Photonic generation of ultra-wideband signals via pulse compression in a highly nonlinear fiber*, IEEE Photonics Technology Letters **22**(4), 2010, pp. 239–241.

[21] ZENG F., WANG Q., YAO J., *All-optical UWB impulse generation based on cross-phase modulation and frequency discrimination*, Electronics Letters **43**(2), 2007, pp. 121–122.

[22] VELANAS P., BOGRIS A., ARGYRIS A., SYVRIDIS D., *High-speed all-optical first- and second-order differentiators based on cross-phase modulation in fibers*, Journal of Lightwave Technology **26**(18), 2008, pp. 3269–3276.

[23] ENBO ZHOU, XING XU, LUI K.S., WONG K.K.Y., *Photonic ultrawideband pulse generation with HNL-DSF-based phase and intensity modulator*, IEEE Photonics Technology Letters **23**(7), 2011, pp. 396–398.

[24] WEI LI, LI XIAN WANG, HOFMANN W., NING HUA ZHU, BIMBERG D., *Generation of ultra-wideband triplet pulses based on four-wave mixing and phase-to-intensity modulation conversion*, Optics Express **20**(18), 2012, pp. 20222–20227.

[25] LIANG ZHAO, JUNQIANG SUN, DEXIU HUANG, *Photonic generation of ultrawideband signals by exploiting gain saturation of dark pump pulse with double undershoots in a highly nonlinear fiber*, Optics Communications **284**(6), 2011, pp. 1669–1676.

[26] YOU MIN CHANG, JUNSU LEE, JU HAN LEE, *Bismuth nonlinear optical fiber for photonic ultrawideband radio-signal processing*, IEEE Journal of Selected Topics in Quantum Electronics **18**(2), 2012, pp. 891–898.

[27] KANG TAN, MARPAUNG D., RAVI PANT, FENG GAO, ENBANG LI, JIAN WANG, DUK-YONG CHOI, MADDEN S., LUTHER-DAVIES B., JUNQIANG SUN, EGGLETON B.J., *Photonic-chip-based all-optical ultra-wideband pulse generation via XPM and birefringence in a chalcogenide waveguide*, Optics Express **21**(2), 2013, pp. 2003–2011.

[28] LIU F., WANG T., ZHANG Z., QIU M., SU Y., *On-chip photonic generation of ultra-wideband monocycle pulses*, Electronics Letters **45**(24), 2009, pp. 1247–1249.

[29] ROELOFFZEN C.G.H., LEIMENG ZHUANG, TADDEI C., LEINSE A., HEIDEMAN R.G., VAN DIJK P.W.L., OLDENBEUVING R.M., MARPAUNG D.A.I., BURLA M., BOLLER K.-J., *Silicon nitride microwave photonic circuits*, Optics Express **21**(19), 2013, pp. 22937–22961.

[30] CHAO WANG, FEI ZENG, JIANPING YAO, *All-fiber ultrawideband pulse generation based on spectral shaping and dispersion-induced frequency-to-time conversion*, IEEE Photonics Technology Letters **19**(3), 2007, pp. 137–139.

[31] ZHAN-QIANG HUI, JIAN-GUO ZHANG, *Wavelength conversion, time demultiplexing and multicasting based on cross-phase modulation and four-wave mixing in dispersion-flattened highly nonlinear photonic crystal fiber*, Journal of Optics **14**(5), 2012, article 055402.

[32] RUSSELL P., *Photonic crystal fiber*, Science **299**(5605), 2003, pp. 358–362.

[33] FEI WANG, JIANJI DONG, ENMING XU, XINLIANG ZHANG, *All-optical UWB generation and modulation using SOA-XPM effect and DWDM-based multi-channel frequency discrimination*, Optics Express **18**(24), 2010, pp. 24588–24594.

[34] XIAO-HUI LI, YONG-GANG WANG, YI-SHAN WANG, XIAO-HONG HU, WEI ZHAO, XIANG-LIAN LIU, JIA YU, CUN-XIAO GAO, WEI ZHANG, ZHI YANG, CHENG LI, DE-YUAN SHEN, *Wavelength-switchable and wavelength-tunable all-normal-dispersion mode-locked Yb-doped fiber laser based on single--walled carbon nanotube wall paper absorber*, IEEE Photonics Journal **4**(1), 2012, pp. 234–241.

[35] LI X.H., WANG Y.S., ZHAO W., ZHANG W., YANG Z., HU X.H., WANG H.S., WANG X.L., ZHANG Y.N., GONG Y.K., LI C., SHEN D.Y., *All-normal dispersion, figure-eight, tunable passively mode-locked fiber laser with an invisible and changeable intracavity bandpass filter*, Laser Physics **21**(5), 2011, pp. 940–944.
[36] XIAOHUI LI, XUEMING LIU, DONG MAO, XIAOHONG HU, HUA LU, *Tunable and switchable multiwavelength fiber lasers with broadband range based on nonlinear polarization rotation technique*, Optical Engineering **49**(9), 2010, article 094303.
[37] SUN M., LONG J.Y., LI X.H., LIU Y., MA H.F., AN Y., HU X.H., WANG Y.S., LI C., SHEN D.Y., *Widely tunable Tm:LuYAG laser with a volume Bragg grating*, Laser Physics Letters **9**(8), 2012, pp. 553–556.
[38] BO MENG, JIN TAO, XIAO HUI LI, YONG QUAN ZENG, SHENG WU, QI JIE WANG, *Tunable single-mode slot waveguide quantum cascade lasers*, Applied Physics Letters **104**(20), 2014, article 201106.

Received August 22, 2014
in revised form November 16, 2014